Transition from ballistic to electrodiffusive transport in free-standing nanometer-sized polymer membranes

Susanne Schulze and Karl-Michael Weitzel
Fachbereich Chemie, Philipps-Universität Marburg, Marburg, Germany
(Received 4 March 2015; revised manuscript received 4 September 2015; published 30 November 2015)

The transition from ballistic to electrodiffusive transport of ions through thin polymer membranes has been investigated by recording single transport events via time-correlated single-particle detection. At the highest kinetic energies investigated, ballistic transport of potassium ions is observed with no discernible energy loss to the membrane. At the lowest kinetic energies investigated (several 100 eV) ions are demonstrated to lose the entire kinetic energy to the membrane. Transport there occurs by electrodiffusion. A transition regime is observed. The transition energy is shown to depend on the thickness of the membrane.

DOI: 10.1103/PhysRevE.92.052602 PACS number(s): 73.61.Ph, 66.30.H−, 66.10.cd, 66.10.cg

I. INTRODUCTION

The transport of electrically charged particles, in particular cations, through thin membranes is of significant interest in biophysics, sensorics, and energy storage. Porous ion-exchange membranes are for instance routinely used in separation processes in both chemical and medical applications [1–3]. These membranes are formed from polymers with charged groups and therefore they are selectively permeable for either cations or anions. The ion-exchange membranes play a vital role in fuel cells [4,5], batteries [6], and sensors [7–12], where they act as either mediators or barriers for the ion transport. Furthermore, biological membranes enable transport processes in the human body; the transport of potassium and sodium ions through selective ion channels is the basis for signal transport through cell membranes. The bombardment of thin films by low-energy ion beams provides access to information on the binding situation in such materials. For example, the bombardment of graphene with B, N, and F ions of energy below 35 eV affects the chemical binding in the graphene layer [13]. Bombardment of amorphous $Zr_{65}Al_{7.5}Cu_{27.5}$ films with keV Kr ion beams leads to surface smoothing reflecting the contribution from surface diffusion but also ballistic effects [14,15].

A more fundamental aspect of transport processes pertains to the scaling laws for the mean displacement of the transport quantity. For mass transport, i.e., "normal" diffusion, the mean square displacement $\langle x^2 \rangle$, scales linearly with time. A deviation from this behavior is often termed "anomalous diffusion" [16,17]. A pragmatic approach to classifying mass transport is based on the proportionality $\langle x^2 \rangle \sim t^n$, where n is a parameter with $n \geqslant 0$ [18]. Often only the range $0 \leqslant n \leqslant 2$ is considered. Here, the regime $n \leqslant 1$ is termed subdiffusive; the regime $n \geqslant 1$ is termed superdiffusive. Subdiffusion is often observed in confined geometries, e.g., in channels with characteristic particle-particle interactions [19]. In lithium metaphosphate glasses the spatial extent of subdiffusion of lithium ions has been correlated with the average size of cages between percolation barriers caused by the glass network [20]. Lithium ion transport has been shown to be subdiffusive on time scales shorter than 10^{-2} s in dilithium ethylene dicarbonate [21]. The most classical case of superdiffusion—from our perspective—is ballistic transport, where the mean square displacement scales as $\langle x^2 \rangle \sim t^2$. It seems worth mentioning that in pioneering work Richardson investigated the spatial distribution of smoke in the atmosphere. He reported that the squared variation of nearest-neighbor separation scales as $\sigma \sim t^3$, which is today sometimes considered an early example of anomalous diffusion [22]. A prominent class of superdiffusive transport processes is the Lévy flight, for which the exponent n is in the range $1 < n < 2$, e.g., for the laminar flow of tracer particles [23]. There is considerable effort in understanding the transition between the different transport regimes mentioned above. There are reports on the time dependence of transport characteristics, where transport is subdiffusive at short times but superdiffusive at longer times; see, e.g., [24]. A special case of subdiffusion is the so-called single-file diffusion (SFD) which is relevant for transport in ion channels. Sane *et al.* reported the transition from SFD, where $\langle x^2 \rangle \sim t^{0.5}$, to regular (Fickian) diffusion, where $\langle x^2 \rangle \sim t$ [25].

Conceptually there must be a transition from diffusive to ballistic transport under certain experimental conditions. However, to the best of our knowledge a clear demonstration of such a transition from diffusive to ballistic transport has not apparently been reported in the literature so far. Evidently examples for superdiffusion have in general been observed in gaseous media; examples for subdiffusion on the other hand have been reported in solid media. This seems to suggest that the best conditions for identifying the transition may be met in soft matter, possibly a thin polymer film.

One of the ingredients for understanding the transport characteristics concerns the balance of energy. Clearly, a fast bullet is supposed to penetrate a sheet of paper without significant loss of kinetic energy (neglecting frictional losses). Similarly a fast ion beam will penetrate a thin polymer membrane provided the kinetic energy is high enough. On the other hand a thermal ion beam may attach to the surface of the membrane via soft landing. Subsequently the ions may diffuse through the membrane, reach the back side of the membrane, and eventually leave it. In the current work we will present the results of an investigation where the transport characteristics of a pulsed ion beam through a polymer membrane of several 100 nm thickness is investigated as a function of the kinetic energy of the ion beam. We will demonstrate that at high kinetic energy ions do not lose energy to the membrane; at lower kinetic energy (but still far above the thermal regime) they lose basically the entire kinetic energy to the membrane.

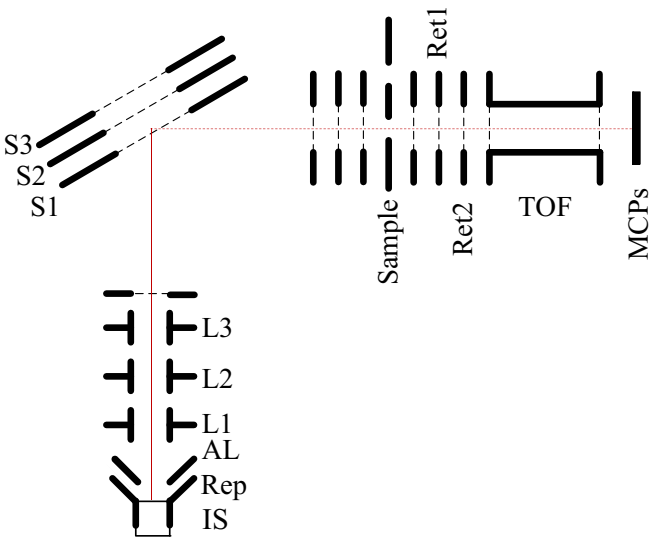

FIG. 1. (Color online) Sketch of the experimental setup containing the ion source (IS), the repeller lens (Rep), the abstraction lens (AL), the lenses (L1–L3), the electric mirror (S1–S3), and the free-standing PPX sample and the acceleration lenses (Ret1 and Ret2), the flight tube (TOF), and the detector (MCPs). The path of the ion beam is indicated by a solid line (continous beam) from the IS to the pulsed mirror and a dashed line (pulsed beam) from there to the detector.

As a measure of energy dissipation we take the time of flight of individual ions "flying" through the polymer membrane.

II. EXPERIMENTAL SETUP

The transport of potassium ions through free standing poly(*para*-xylylene) (PPX) membranes is investigated in an ultrahigh-vacuum chamber operated at a pressure of $p < 10^{-8}$ mbar. The setup consists of three different regions: the ionization chamber, the pulsing chamber, and the sample chamber. These components are schematically illustrated in Fig. 1.

The continuous ion beam is generated by thermionic emission of potassium ions from synthetic leucite $K[AlSi_2O_6]$. Leucite is produced by tempering K_2CO_3, Al_2O_3, and SiO_2 in a molar ratio of 1:1:4. It is mixed with molybdenum powder in a ratio of 1:4 to optimize the heat flow through the emitter and to ensure that the material shows a homogeneous temperature. The mixture is pressed into a steel pot and tempered in vacuum ($p = 10^{-6}$ mbar) with a temperature of 1200 °C for 12 h. The steel pot containing the leucite is welded onto a device that allows the material to be heated.

In the experiment, the potassium ions are emitted from the top of the ion source. For all experiments described in this paper a heating current of 3.2 A is applied to the emitter. The potassium ions leaving the emitter are repelled by a positive voltage applied to the repeller lens (Rep) and accelerated towards the abstraction lens. The voltage applied to the repeller defines the kinetic energy of the ions. In the experiments described in this paper, the repeller voltage is varied between 500 and 2200 V. To adjust the ion beam position in the x and y directions static voltages between 0 and ±300 V are applied to the two half lenses L1 and L2. Lens L3 and the aperture with an electroformed copper mesh (transmission of 95%) on the central opening are set to ground potential to ensure a well-defined field in front of the mirror in the pulsing chamber. After passing the aperture the ion beam enters the pulsing chamber. In its middle an electric mirror, consisting of three lenses S1, S2, and S3 with an angle of 45° towards the propagation axis of the ion beam, is fixed. By applying a pulsed voltage to lens S2, an ion pulse is created. To obtain these ion pulses, a TTL (Transistor-Transistor Logic)-pulse with a width of 1 µs is used as a control signal for a high-voltage transistor switch (Behlke HTS 31-GSM). The leading and trailing edges switch the positive voltage at S2 on and off. The applied positive voltage has the same value as U_{Rep} and the pulse repetition rate is 15 kHz. The ion pulses thus generated enter the sample chamber, where each lens has identical central bores of a diameter of 1 mm; these bores are covered with high-transmission electroformed meshes to ensure that that no external electric field gradients exists. After the mirror the ions pass three grounded copper lenses before arriving at the sample holder. The sample holder has two identical bores; one of the two is covered with the polymer membrane while the other remains open. Thus it is possible to easily change between sample and reference measurements. Another copper lens is mounted 8 mm behind the sample. The sample mount and the two engirding lenses are set to ground potential. This ensures that the membrane does not experience any external electric field gradient.

Ions transmitted through the membrane are accelerated towards another electrostatic lens Ret1 covered by a mesh set to a potential of −1000 V. Subsequently the ions pass an electrostatic lens Ret2 and a time-of-flight tube (TOF) operated at a potential of −2400 V. Finally the ions are detected by a pair of microchannel plates (MCPs) in chevron arrangement [18]. The MCP detector has a time resolution on the order of a few nanoseconds. An amplifier/discriminator (Ortec 9302) is employed to convert the MCP signal into a negative standard NIM (Nuclear-Instrumentation Module) signal. This signal is used as the STOP signal for a time-to-amplitude converter TAC (Ortec TAC/SCA 567) with a time range of 50 µs. A TAC operates by receiving two input pulses, called START and STOP, and then outputting a pulse, the amplitude of which is proportional to the time interval between the rising edge of the START and STOP signals. The start signal for the TAC is obtained by using a TTL signal having the same starting time as the pulse for the Behlke switch. To measure the time-of-flight-mass spectra (TOF spectra) the TAC output pluses are passed to a multichannel buffer (Ortec 926 ADCAM MCB) that converts the analog output pulse with an analog-to-digital (A-D) converter into its digital equivalent and saves it internally into 8192 channels leading to an initial bin width of 6.1 ns/channel. These data are transferred via a USB interface and processed in the program MAESTRO 32 installed on a personal computer. Ultimately, for presentation the TOF data covering 50 µs are bundled into 512 bins leading to a final bin width of 97.66 ns/bin.

The samples investigated are membranes of the polymer poly(*para*-xylylene) with a thickness of 830 nm ± 15 nm and 1.30 µm ± 20 nm. The membrane thickness is determined by profilometry. PPX films are prepared by chemical vapor

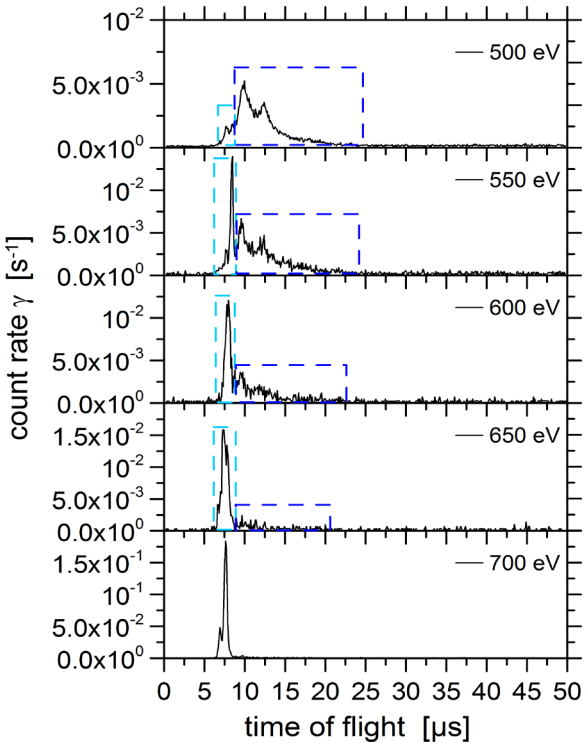

FIG. 2. (Color online) Time of flight through an 830 nm PPX membrane for kinetic energies of the potassium ions of 500–700 eV. The light (left) and dark (right) blue rectangles are used to indicate the two regions of interest observed for the ion transport through the membrane.

deposition via the Gorham process [26]. To this end *para*-cyclophane is pyrolyzed at 650 °C and approximately 1 mbar. The reactive intermediates are deposited at room temperature onto a quartz slide. Finally the membrane is transferred to one of the two bores of the slidelike copper plate already described above. It is this region of the sample which constitutes a free-standing membrane. More details have been reported in Refs. [27,28]. Throughout this work we use the term membrane as a synonym for a "free-standing polymer membrane."

III. RESULTS AND DISCUSSION

The time-correlated transport of potassium ions through a free-standing PPX membrane with a thickness of 830 nm and one with a thickness of 1.30 µm was investigated for kinetic energies of the ions between 500 and 2200 eV. As a first result we present the time-of-flight spectra for ions being transported through the 830 nm PPX-membrane (Fig. 2). For all energies up to 650 eV the spectra show two different peaks in the TOF spectra as marked by light blue (left) and dark blue rectangles (right) in Fig. 2. For the lowest energy depicted here, the second peak is more dominant with a maximum count rate of $5.2 \times 10^{-3}\,\mathrm{s}^{-1}$ and time of flight of 9.95 µs, whereas the first peak with a flight time of 7.70 µs and a maximum count rate of $1.6 \times 10^{-3}\,\mathrm{s}^{-1}$ is significantly smaller. These two peaks indicate that there have to be two different transport processes taking place at the same time. The first peak accounts for ions that exit the membrane with the same energy as they

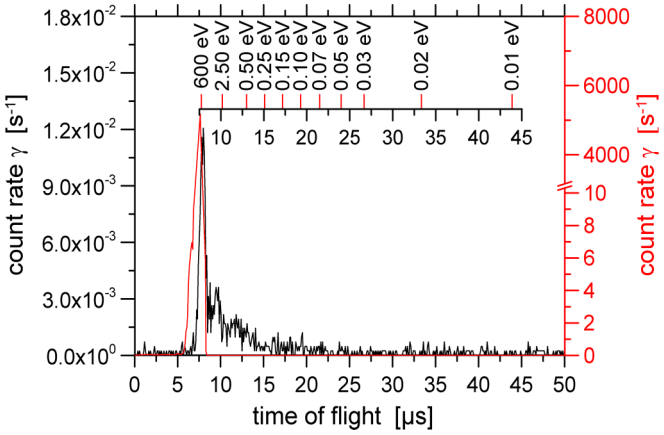

FIG. 3. (Color online) Kinetic energy analysis of an 830 nm PPX membrane for an initial energy of 600 eV. The black trace is the measured spectrum with the membrane. The red time-of-flight spectrum (the first large peak) is a reference spectrum without the membranes in the beam's pass.

impinged on it as seen in the reference spectrum [red (gray) in Fig. 3]. This type of energy-lossless transport is comparable to the ballistic transport seen in electron gases [29]. The second peak is caused by ions that have a smaller energy than the initial ions, indicating that an electrodiffusive mechanism is responsible for this kind of ion transport.

Increasing the kinetic energy of the ions by 50 eV to 550 eV, one observes a steep growth of the first peak, the count rate for which is now $\gamma = 1.4 \times 10^{-2}\,\mathrm{s}^{-1}$, and a smaller growth in the count rate of the second peak ($\gamma = 6.6 \times 10^{-3}\,\mathrm{s}^{-1}$). Comparison of the count rates for energies of 550 and 600 eV shows that the count rate of the second peak starts to decrease and only 54 % of the peak area is thus caused by this kind of transport. Therefore in this energy range a significant change in the transport is observed. For higher energies the ballistic transport mechanism is clearly favored. This claim is strengthened by the time-of-flight spectra for ion energies of 650 and 700 eV; here the peak caused by a ballistic ion transport has a maximum count rate of $\gamma_{\mathrm{bal,\,650\,eV}} = 1.6 \times 10^{-2}\,\mathrm{s}^{-1}$ and $\gamma_{\mathrm{bal,\,700\,eV}} = 1.8 \times 10^{-1}\,\mathrm{s}^{-1}$ and the electrodiffusive peak starts to vanish ($\gamma_{\mathrm{dif,\,650\,eV}} = 2.4 \times 10^{-3}\,\mathrm{s}^{-1}$, $\gamma_{\mathrm{dif,\,700\,eV}} = 4.2 \times 10^{-3}\,\mathrm{s}^{-1}$). Even though the count rate for the diffusive peak maximum is slightly increased for an energy of 700 eV, the peak area is decreasing. This behavior indicates that the transport is strongly dependent on the energy.

The time of flight of the ballistic peak in general decreases with increasing kinetic energy of the ion beam, as would be expected for a ballistic process. Note, however, that this total TOF does not originate only from a drift region but also from acceleration and deceleration regions; it also contains an electronic offset. We will discuss the actual TOFs in some more detail below.

To obtain further information on the energy distribution in the TOF spectra we performed a kinetic energy analysis. Figure 3 show this analysis for an impact energy of 600 eV both with the membrane present (black curve) and without the membrane in the beam path [the grey (red) peak].

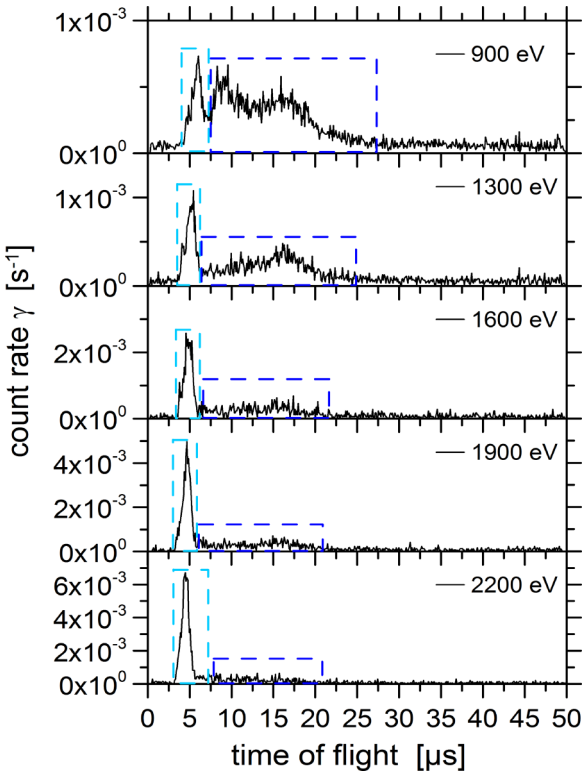

FIG. 4. (Color online) TOF spectra for a free-standing 1.3 µm PPX membrane. The light (left) and dark (right) blue rectangles are used to indicate the two regions of interest observed for the ion transport through the membrane.

As one would expect, the reference measurement shows that the ions in the absence of the membrane exhibit a flight time that is theoretically calculated for ions having energies of 600 eV taking into account the full geometry of the spectrometer. If, however, the membrane is placed in the beam path, this situation changes drastically. Now we obtain a two-peak spectrum, where only the first peak accounts for ions having the same energy as in the initial reference experiment. The second peak caused by potassium ions with a time of flight between 8.78 and 25.56 µs accounts for ions leaving the membrane with kinetic energies ranging from 125 eV to 40 meV. Thus, these ions are significantly slowed down, but only a small fraction of the ions leaves the membrane with thermal energy. The finding of ions with lower kinetic energy than the initial energy is an indicator of an electrodiffusive transport mechanism.

To further investigate the transport properties and their dependence not only on the impact energy but also on the thickness of the free-standing PPX membrane, we examined a membrane with a thickness of 1.3 µm (Fig. 4). For a kinetic energy of 900 eV the time of flight for the peak maximum of the ballistic ions [light blue (left) rectangle] is $t = 6.04$ µs with a count rate of $\gamma_{\mathrm{bal}} = 7.0 \times 10^{-4}\,\mathrm{s}^{-1}$ and the electrodiffusive TOF is 9.56 µs with a count rate of $\gamma_{\mathrm{dif}} = 6.4 \times 10^{-4}\,\mathrm{s}^{-1}$. Increasing the impact energy to 1300 eV shows a decrease in the electrodiffusive peak [dark blue (right) rectangle, $\gamma_{\mathrm{dif}} = 4.4 \times 10^{-4}\,\mathrm{s}^{-1}$] and simultaneously an increase in the peak caused by ballistic ions ($\gamma_{\mathrm{bal}} = 1.0 \times 10^{-3}\,\mathrm{s}^{-1}$). For an

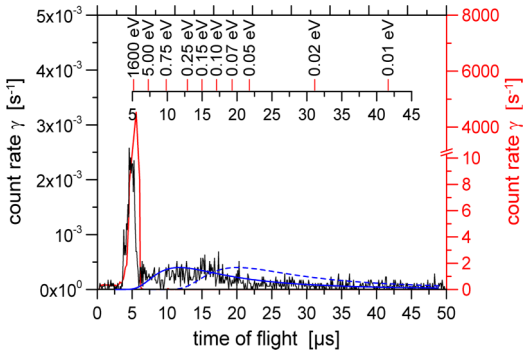

FIG. 5. (Color online) Kinetic energy analysis for an impact energy of 1600 eV. The red curve shows the reference measurement. The black curve is the spectrum for a 1.3 µm PPX membrane. The blue lines are the result of simulations based on $\langle\varepsilon\rangle = 39$ meV (dashed) and $\langle\varepsilon\rangle = 78$ meV (solid).

impact energy of 1600 eV the ballistic ions show a count rate of $\gamma_{\mathrm{bal}} = 2.5 \times 10^{-3}\,\mathrm{s}^{-1}$ at a flight time of $t = 4.58$ µs and the electrodiffusive peak exhibits a count rate of $\gamma_{\mathrm{dif}} = 6.4 \times 10^{-4}\,\mathrm{s}^{-1}$ at its maximum. The TOF spectrum for ions with an energy of 1900 eV shows a two-peak spectrum having times of flight of $t = 4.68$ and 14.93 µs. These two peaks can be attributed to a ballistic and an electrodiffusive transport process, even though the diffusive pulse exhibits only a low signal intensity ($\gamma_{\mathrm{dif}} = 6.6 \times 10^{-4}\,\mathrm{s}^{-1}$) compared to the ballistic peak ($\gamma_{\mathrm{dif}} = 4.9 \times 10^{-3}\,\mathrm{s}^{-1}$). If the impact energy is increased to 2200 eV the TOF for the ballistic signal decreases further ($t = 4.48$ µs) and the count rate increases to $\gamma_{\mathrm{bal,\,650\,eV}} = 6.7 \times 10^{-3}\,\mathrm{s}^{-1}$.

What becomes apparent when we compare the ballistic count rates for the 1.3-µm-thick membrane with the 830 nm sample is a slower growth of the count rate for the thicker membrane. The electrodiffusive peak for an impact energy of 2200 eV has a maximum count rate of $\gamma_{\mathrm{dif}} = 6.2 \times 10^{-4}\,\mathrm{s}^{-1}$ and is therefore only slightly visible in the TOF spectrum. This behavior of the vanishing electrodiffusive transport indicates that this membrane, like the 830 nm membrane, shows a strong dependence of the transport mechanisms on the impact energy of the ions.

Figure 5 shows the TOF spectra for kinetic energies of 1600 eV for potassium ions transported through the membrane (black curve) and ions without the membrane in the beam path [red (gray) curve]. The kinetic energy for the red (gray) curve and the first peak of the PPX measurement are in good agreement with the ions having a kinetic energy of 1600 eV. This ion peak thus originates from ions being transported ballistically through the membrane. The energies of the second ion peak in the TOF spectrum were calculated to be in the range of thermal energy up to around 5 eV, therefore indicating that a diffusive process is responsible for this kind of transport through the membrane. In order to further analyze the energy distribution of the ions contributing to this transport process we have performed additional simulations. These simulations start from an energy distribution given by

$$P(\varepsilon_i) = P_o \exp\left[-\varepsilon_i/\langle\varepsilon\rangle\right], \tag{1}$$

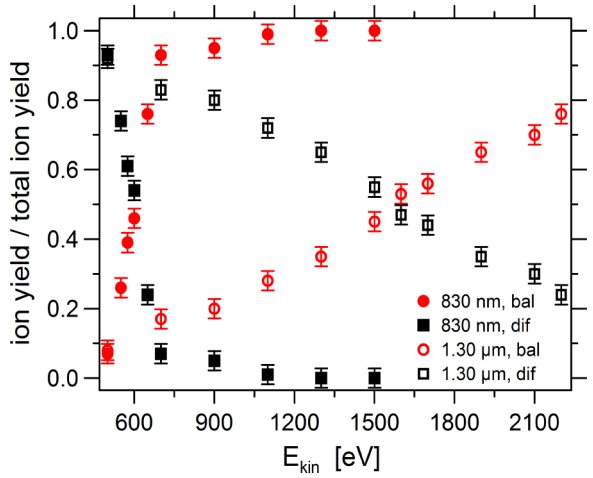

FIG. 6. (Color online) The ion yield for both PPX membranes as a function of the kinetic energy of the impinging ions. The error bars indicate the estimated uncertainty of ±3% based on the variation of the relative ion yields with time.

where ε_i is the energy of the particle, $\langle\varepsilon\rangle$ is the average energy of the ensemble, and P_o is a normalization constant. This probability distribution has to be transformed from the energy domain into the time-of-flight (τ) domain by

$$P'(\tau_i) = P(\varepsilon_i)\partial\varepsilon/\partial\tau. \tag{2}$$

The result of such simulations is shown in Fig. 5 as blue lines for two different average energies. The dashed blue line corresponds to an average energy of 39 meV [$(3/2)kT$ at room temperature], while the solid blue line corresponds to an average energy of 78 meV. Evidently the latter simulation is in reasonable agreement with the experimental data. It seems worthwhile to emphasize that the maximum of the probability distribution in the TOF domain appears at a TOF which corresponds to an energy larger than that energy for which the maximum appears in the energy domain. This is the inherent result of the transformation given in Eq. (2). The pivotal conclusion from this analysis is that the ions contributing to this slow part of the signal are characterized by an average energy which is only to a minor extent larger than true thermal conditions. Note that under the experimental conditions chosen electric stray fields can easily affect the kinetic energy of charged particles by some 10 meV. In fact the simulations show that stray fields have apparently been quite effectively reduced in our setup. Ultimately we will concentrate on the relative yields from the quasiballistic and the diffusive contributions to the total TOF distributions.

Both membrane thicknesses indicate that for a pulsed ion beam both an electrodiffusive and a ballistic transport process have to be considered.

The difference between these two thicknesses becomes apparent when one considers the ion yield for each peak versus the total ion yield (Fig. 6). The 830-nm-thick membrane shows a very steep incline in the ballistic ion yield at very low kinetic energies, and the point where the ion yields for both the electrodiffusive (black filled squares) and the ballistic (red filled circles) transport process are the same (crossover point) is reached at approximately 600 eV. The 1.3 µm PPX membrane shows a slower increase over a larger kinetic energy interval in the ballistic ion yield (red open circles). The thicker membrane exhibits the crossover point at approx. 1550 eV. So increasing the membrane thickness by 500 nm moves the crossover point by 950 eV. Not only is the crossover point shifted, but the increase in the peak caused by ballistically transported ions is slower for the thicker PPX sample. So in the energy range investigated in this paper only the thinner sample shows a ballistic ion yield of 100%, whereas for the thicker sample the maximum ballistic yield is 78% and the electrodiffusive yield (black open squares) is 22%. This behavior could be attributed to the fact, that due to the bigger membrane thickness the count rate of the diffusive peak (Fig. 4) decreases slower and therefore the diffusive part of the transport is still more dominant. Therefore it can be concluded that by looking at the transport characteristics it is possible to analyze the thickness of PPX membranes and also to show that there is a thickness dependent transition from the electrodiffusive transport to the ballistic transport.

Recent papers have shown that ballistic electron transport is actually a quite common phenomena in both doped and pure graphenes [30,31]. Baringhaus *et al.* found that 40-nm-wide graphene ribbons epitaxially grown on silicon carbide are room-temperature ballistic conductors over a length scale greater than ten microns [31]. This length scale is comparable to the thickness of our PPX membranes and therefore shows that ballistic transport is possible even for such long distances. When talking about ballistic transport in connection with the results shown here it is important to keep in mind that the measurements described in this paper enable us to compare energies with or without the membrane in the beam's pass. We cannot distinguish between an impinging ion being immediately and ballistically transported through the membrane and an impinging ion, which through elastic scattering forces an ion that was already present in the membrane out of it.

IV. SUMMARY

The transport characteristics for potassium ions in a thin PPX polymer membrane have been investigated by bombarding the membrane with a beam of K^+ ions of well-defined kinetic energy. The attachment of alkali-metal ions to the front side of the membrane leads to a surface potential as defined by the source potential of the ion beam. Single transport events have been recorded by time-correlated detection of single ions behind the membrane. The start signal for the time correlation is defined by an electric field pulse which enforces a chopping of the ion beam.

At the highest kinetic energies investigated (> 1000 V) ballistic transport of potassium ions is observed with no discernible energy loss to the membrane. At the lowest kinetic energies investigated (several 100 eV) ions are demonstrated to lose the entire kinetic energy to the membrane. Transport there occurs by electrodiffusion. Thus, the current work has demonstrated the transition from ballistic to electrodiffusive transport as the impact energy decreases. The transition energy is observed to depend on the membrane thickness; the thicker the membrane the higher the kinetic energy required to induce ballistic transport.

[1] W. Kujawski, M. Staniszewski, and T. Nguyen, Transport parameters of alcohol vapors through ion-exchange membranes, Sep. Purif. Technol. **57**, 476 (2007).
[2] W. Mabrouk, L. Ogier, S. Vidal, C. Sollogoub, F. Matoussi, and J. F. Fauvarque, Ion exchange membranes based upon crosslinked sulfonated polyethersulfone for electrochemical applications, J. Membr. Sci. **452**, 263 (2014).
[3] U. Kuhlmann, R. Gräf, J. Schindler, and H. Lange, Continuous ionography (CIG) in haemodialysis by ion-selective carrier membrane electrodes (ISCME) with solid cement contact for flow-through measurement, Int. J. Artif. Organs **15**, 208 (1992).
[4] H. Zhang and P. K. Shen, Recent development of polymer electrolyte membranes for fuel cells, Chem. Rev. **112**, 2780 (2012).
[5] L. C. Pérez, L. Brandão, J. M. Sousa, and A. Mendes, Segmented polymer electrolyte membrane fuel cells—A review, Renewable Sustainable Energy Rev. **15**, 169 (2011).
[6] P. Knauth, Ionic conductor composites: Theory and materialsg, J. Electroceram. **5**, 111 (2000).
[7] B. Ding, M. Wang, X. Wang, J. Yu, and G. Sun, Electrospun nanomaterials for ultrasensitive sensors, Mater. Today **13**, 16 (2010).
[8] J. Bobacka, Conducting polymer-based solid-state ion-selective electrodes, Electroanalysis **18**, 7 (2006).
[9] A. Meller, L. Nivon, E. Brandin, J. Golovchenko, and D. Branton, Rapid nanopore discrimination between single polynucleotide molecules, Proc. Natl. Acad. Sci. USA **97**, 1079 (2000).
[10] O. Shekhah, J. Liu, R. A. Fischer, and C. Wöll, MOF thin films: Existing and future applications, Chem. Soc. Rev. **40**, 1081 (2011).
[11] R. K. Nagarale, G. S. Gohil, and V. K. Shahi, Recent developments on ion-exchange membranes and electro-membrane processes, Adv. Colloid Interface Sci. **119**, 97 (2006).
[12] R. Knake, P. Jacquinot, and P. C. Hauser, A direct comparison of amperometric gas sensors with gas-diffusion and ion-exchange membrane based electrodes, Analyst **127**, 114 (2002).
[13] Y. Xu, K. Zhang, C. Brüsewitz, X. Wu, and H. C. Hofsäss, Investigation of the effect of low energy ion beam irradiation on mono-layer graphene, AIP Adv. **3**, 072120 (2013).
[14] S. Vauth and S. G. Mayr, Relevance of surface viscous flow, surface diffusion, and ballistic effects in keV ion smoothing of amorphous surfaces, Phys. Rev. B **75**, 224107 (2007).
[15] S. Vauth and S. G. Mayr, Ion bombardment induced smoothing of amorphous metallic surfaces: Experiments versus computer simulations, Phys. Rev. B **77**, 155406 (2008).
[16] J.-P. Bouchaud and A. Georges, Anomalous diffusion in disordered media: Statistical mechanisms, models and physical applications, Phys. Rep. **195**, 127 (1990).
[17] I. Eliazar and J. Klafter, Anomalous is ubiquitous, Ann. Phys. (NY) **326**, 2517 (2011).
[18] I. Eliazar and J. Klafter, A probabilistic walk up power laws, Phys. Rep. **511**, 143 (2012).
[19] P. S. Burada, P. Hanggi, F. Marchesoni, G. Schmid, and P. Talkner, Diffusion in confined geometries, ChemPhysChem **10**, 45 (2009).
[20] A. Shaw and A. Ghosh, Correlation of microscopic length scales of ion dynamics with network structure in lithium-iodide-doped lithium metaphosphate glasses, EPL **100**, 66003 (2012).
[21] O. Borodin, G. R. V. Zhuang, P. N. Ross, and K. Xu, Molecular dynamics simulations and experimental study of lithium ion transport in dilithium ethylene dicarbonate 2, J. Phys. Chem. C **117**, 7433 (2013).
[22] J. H. Cushman, D. O'Malley, and M. Park, Anomalous dispersion, renormalization groups, scaling laws and classification: A reflection on recent efforts, Adv. Water Resour. **62**, 207 (2013).
[23] T. H. Solomon, E. R. Weeks, and H. L. Swinney, Observation of Anomalous Diffusion and Lévy Flights in a Two-Dimensional Rotating Flow, Phys. Rev. Lett. **71**, 3975 (1993).
[24] A. W. Harrison, D. A. Kenwright, T. A. Waigh, P. G. Woodman, and V. J. Allan, Modes of correlated angular motion in live cells across three distinct time scales, Phys. Biol. **10**, 036002 (2013).
[25] J. Sane, J. T. Padding, and A. A. Louis, The crossover from single file to Fickian diffusion, Faraday Discuss. **144**, 285 (2010).
[26] W. F. Gorham, A new, general synthetic method for the preparation of linear poly-*p*-xylylenes, J. Polym. Sci., Polym. Chem. Ed. **4**, 3027 (1966).
[27] K. Schroeck, S. Schulze, A. Schlemmer, and K.-M. Weitzel, Time-correlated transport of potassium ions through a thin poly-*p*-xylylene membrane, J. Phys. D: Appl. Phys. **43**, 025501 (2010).
[28] S. Schulze, M. Schaefer, A. Greiner, and K.-M. Weitzel, Bombardment induced ion transport—Part III: Experimental potassium ion conductivities in poly(*para*-xylylene), Phys. Chem. Chem. Phys. **15**, 1481 (2013).
[29] C. Beenakker and H. van Houten, Quantum transport in semiconductor nanostructures, in *Semiconductor Heterostructures and Nanostructures* (Elsevier, Amsterdam, 1991), Vol. 44, p. 1.
[30] H. Khalfoun, A. Lherbier, P. Lambin, L. Henrard, and J.-C. Charlier, Transport regimes in nitrogen-doped carbon nanotubes: Perfect order, semi-random, and random disorder cases, Phys. Rev. B **91**, 035428 (2015).
[31] J. Baringhaus, M. Ruan, F. Edler, A. Tejeda, M. Sicot, A. Taleb-Ibrahimi, A.-P. Li, Z. Jiang, E. H. Conrad, C. Berger, C. Tegenkamp, and Walt A de Heer, Exceptional ballistic transport in epitaxial graphene nanoribbons, Nature (London) **506**, 349 (2014).